nature physics

SUPPLEMENTARY INFORMATION

DOI: 10.1038/NPHYS1363

C. Latta,[1,*] A. Högele,[1,*] Y. Zhao,[2,†] A. N. Vamivakas,[2] P. Maletinsky,[1] M. Kroner,[1] J. Dreiser,[1] I. Carusotto,[3] A. Badolato,[4] D. Schuh,[5] W. Wegscheider,[5,‡] M. Atature,[2] and A. Imamoglu[1]

[1]*Institute of Quantum Electronics, ETH-Zurich, CH-8093, Zurich, Switzerland**

[2]*Cavendish Laboratory, University of Cambridge, JJ Thomson Ave, Cambridge CB3 0HE, UK*

[3]*CNR-INFM BEC Center and Dipartimento di Fisica, Università di Trento, via Sommarive 14, I-38050 Povo, Trento,Italy*

[4]*Department of Physics and Astronomy, University of Rochester, Rochester, New York 14627, USA*

[5]*Institut für Experimentelle und Angewandte Physik, Universität Regensburg, Regensburg, Germany*

(Dated: June 30, 2009)

*These authors contributed equally

†Physikalisches Institut, Ruprecht-Karls-Universitt Heidelberg, Philosophenweg 12, Heidelberg 69120, Germany

‡Solid State Physics Laboratory, ETH Zurich, 8093 Zurich, Switzerland

DOI: 10.1038/NPHYS1363

I. DEPENDENCE OF LASER DRAGGING OF QUANTUM DOT RESONANCES ON EXPERIMENTAL PARAMETERS

The absorption, or equivalently, differential transmission (DT) measurements [1] were performed by setting the gate voltage/laser energy to a specific detuning, waiting for a time T_{dwell} and monitoring the output of the lock-in amplifier. After each measurement, the voltage/laser energy was changed by a detuning step Δ. Figure S1 shows the dependence of the measurement on the parameters T_{dwell} and Δ. The presented data have been taken on the blue Zeeman transition of a neutral sample A QD.

Figure S1a and S1b show DT measurements where the energy detuning was varied in discrete steps of $\Delta = 0.4$ μeV and $\Delta = 1.2$ μeV, respectively. The dwell time T_{dwell} after each step was 200, 1000 and 5000 ms (light to dark grey)corresponding to the lock-in time constant. The energy range where the dynamical nuclear spin polarization (DNSP) effectively compensates for the

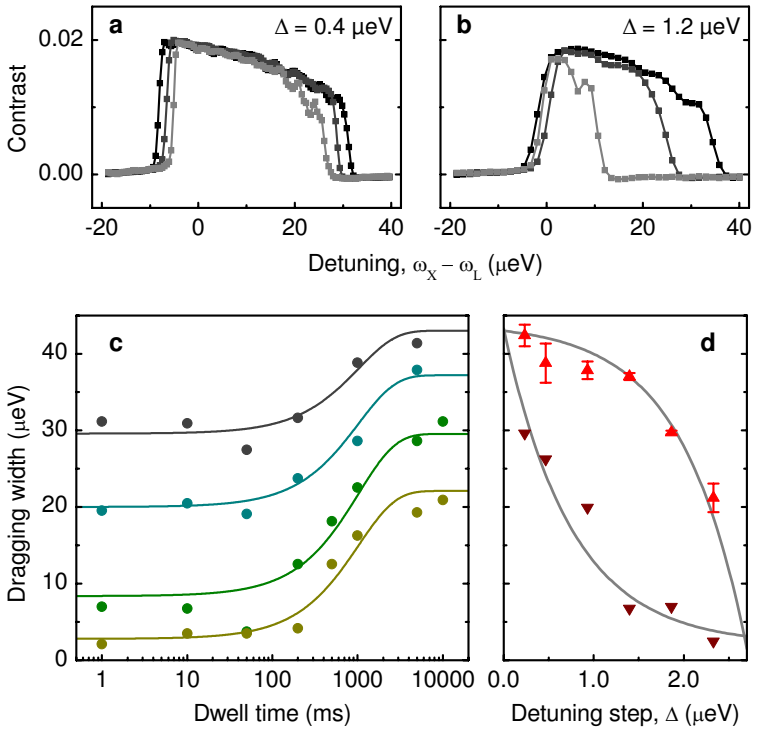

Figure 1: Dragging of the quantum dot resonance as a function of integration time and detuning step size. Absorption scans for different dwell times $T_{\mathrm{dwell}} = 200$, 1000 and 5000ms (light to dark gray) at a given detuning step size of (**a**) $\Delta = 0.4$ μeV and (**b**) $\Delta = 1.2$ μeV. (**c**) Dragging width as function of dwell time T_{dwell} for different detuning steps $\Delta = 0.2, 0.4, 1.6, 2.0$ μeV (from top to bottom). (**d**) Minimum (down-triangles) and maximum (up-triangles) values of the dragging width as a function of detuning step size.

detuning varies drastically with both the step size and the dwell time constant. The dependence of the dragging width on the dwell time is presented in Fig. S1c for fixed detuning steps of $\Delta = 0.2, 0.4, 1.6$ and 2.0 μeV (from top to bottom). In two limiting cases, namely for short and long time constants, the dragging width becomes independent of $T_{\rm dwell}$ and saturates at minimum/maximum values. The solid lines are saturation fits to each set of data with a common fitting parameter $\tau = (1.0 \pm 0.3)$ s, a time scale consistent with the characteristic buildup time for DNSP. The minimum (down-triangles) and maximum (up-triangles) values of the dragged resonance are plotted in Fig. S1d along with exponential growth/decay fits as grey solid lines. The fitting parameter here was the critical step size, $\Delta\omega_c = (0.75 \pm 0.05)$ μeV, indicating that the DNSP range reduces exponentially when $\Delta\omega_c \geq \Gamma$.

Figure S2a shows the maximum dragging width at 4.5 T as a function of the laser Rabi frequency Ω_L for the neutral (X^0, circles) and charged (X^-, triangles) exciton in two different sample A QDs. The maximum dragging width is plotted versus the laser Rabi frequency Ω_L, normalized with respect to the linewidth Γ at 0 T. All three sets of data peak around the same value, where $\Omega \simeq \Gamma$. Figure S2b depicts the maximum dragging measured for the neutral exciton as a function of external magnetic field. The sub-linear dependence is apparent when compared to the electron Zeeman splitting $\Delta\omega_z = g_e\mu_B B$ that is a linear function of the external magnetic field (grey solid line). The electron g-factor for this quantum dot ($g_e = -0.67$) was measured by directly pumping the weakly-allowed trion transition ($|\downarrow\rangle \leftrightarrow |\uparrow\downarrow\Uparrow\rangle$) [2].

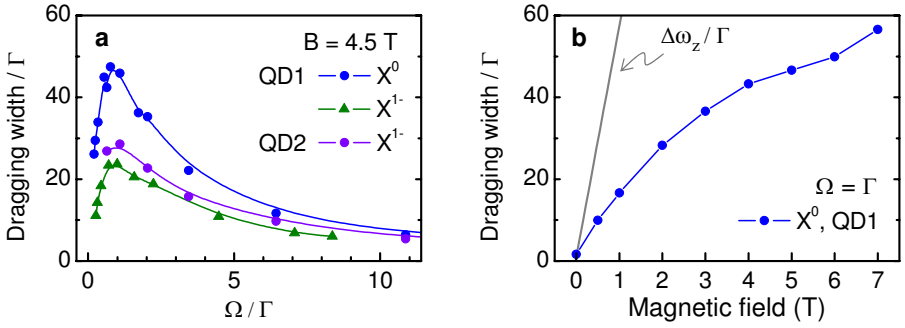

Figure 2: Dependence of the maximum dragging width on laser power and external magnetic field: (**a**) Maximum dragging width (in units of Γ) as a function of laser Rabi frequency for $T_{\rm dwell} = TC = 200$ ms and $\Delta = 0.2$ μeV measured for two different quantum dots QD1 and QD2 in sample A at 4.5 T. Data points for neutral and single-electron charged quantum dots are represented by circles and triangles, respectively. (**b**) Sub-linear growth of the maximum dragging width (in units of Γ) for a fixed laser Rabi frequency $\Omega_{\rm L} = \Gamma$ as a function of external magnetic field (filled circles) plotted along with the linear Zeeman splitting $\Delta\omega_z/\Gamma$ of the electron spin states with $g_e = -0.67$ (grey solid line).

DOI: 10.1038/NPHYS1363

II. THEORETICAL MODEL

We derive a Markovian master equation for the combined system of quantum dot and nuclear spins. In the model we include three states: the two Zeeman split ground states (spin-up electron $|\uparrow\rangle$ and spin-down electron $|\downarrow\rangle$) and the pseudo-spin-up trion state ($|t\rangle = |\uparrow\downarrow\Uparrow\rangle$). The states $|\uparrow\rangle$ and $|t\rangle$ are coherently coupled by a laser field ($\hat{H}_{\rm laser}$) with Rabi frequency Ω_L and photon energy $\hbar\omega_{\rm L}$. Hyperfine interaction ($\hat{H}_{\rm hyp}$) couples the two electron ground states split by energy $\hbar\omega_{\rm z}$, and the nuclear spins. Additionally we include coupling of the blue trion transition ($|\uparrow\rangle \leftrightarrow |\uparrow\downarrow\Uparrow\rangle$) to the reservoir of electric field modes ($\hat{H}_{\rm rad}$) and coupling of the spin transition ($|\uparrow\rangle \leftrightarrow |\downarrow\rangle$) to a low energy reservoir using a spin-boson Hamiltonian ($\hat{H}_{\rm ph}$). $\hat{H}_{\rm ph}$ captures both spin-orbit assisted phonon relaxation and exchange mediated spin-flip co-tunneling events.

The Hamiltonian reads

$$\hat{H} = \underbrace{\hbar\omega_{\rm z}\hat{\sigma}_{\downarrow\downarrow} + \hbar\omega_t\hat{\sigma}_{\rm tt}}_{\hat{H}_0} + \hat{H}_{\rm laser} + \hat{H}_{\rm hyp} + \hat{H}_{\rm rad} + \hat{H}_{\rm ph} \tag{1}$$

where

$$\hat{H}_{\rm laser} = \hbar\Omega_{\rm L}\left(\hat{\sigma}_{\rm t\uparrow}e^{-{\rm i}\omega_{\rm L}{\rm t}} + \hat{\sigma}_{\uparrow{\rm t}}e^{{\rm i}\omega_{\rm L}{\rm t}}\right) \tag{2}$$

$$\hat{H}_{\rm hyp} = \hbar\sum_i A_i(\hat{I}^i_+\hat{\sigma}_- + \hat{I}^i_-\hat{\sigma}_+ + 2\hat{I}^i_{\rm z}\hat{\sigma}_{\rm z}) \tag{3}$$

$$\hat{H}_{\rm rad} = \hbar\sum_k g_k\hat{\sigma}_{\uparrow{\rm t}}\hat{a}^\dagger_k e^{{\rm i}\omega_k{\rm t}} + {\rm h.c.} \tag{4}$$

$$\hat{H}_{\rm ph} = \hbar\sum_q g_q\hat{\sigma}_{\rm z}\left(\hat{b}_q e^{-{\rm i}\omega_q{\rm t}} + \hat{b}^\dagger_q e^{{\rm i}\omega_q{\rm t}}\right) \tag{5}$$

The operators σ_{ij} are defined as $\sigma_{ij} = |i\rangle\langle j|$. A_i is the coupling strength of the electron to the $i-$th nucleus. Coupling of the $|\uparrow\rangle \leftrightarrow |t\rangle$-transition to the $k-$th electric field mode is denoted by g_k. Excitations of electron-hole pairs in the Fermi-sea by exchange interaction or a phonon in the lattice, take place with strength g_q.

For large $\omega_{\rm z}$, flip-flops in the hyperfine interaction do not take place to first order because of energy conservation but could be assisted by spin-preserving co-tunneling or phonon emission/absorption events. To proceed, we eliminate $\sum_i A_i(\hat{I}^i_+\hat{\sigma}_- + \hat{I}^i_-\hat{\sigma}_+)$ to first order by a Schrieffer-Wolff transformation

$$\tilde{H} = e^{\hat{S}}\hat{H}e^{-\hat{S}} = \hat{H} + \left[\hat{S},\hat{H}\right] + \frac{1}{2}\left[\hat{S}\left[\hat{S},\hat{H}\right]\right] + ...$$

with $\hat{S} = \sum_i \frac{A_i}{\omega_{\rm z}}(\hat{I}^i_+\hat{\sigma}_- - \hat{I}^i_-\hat{\sigma}_+)$. The transformed Hamiltonian reads

$$\tilde{H} = \hbar\omega_{\rm z}\hat{\sigma}_{\downarrow\downarrow} + \hbar\omega_t\hat{\sigma}_{\rm tt} + \tilde{H}_{\rm laser} + \tilde{H}_{\rm OH} + \tilde{H}_{\rm rad} + \tilde{H}_{\rm ph} \tag{6}$$

where

$$\begin{aligned}
\tilde{H}_{\mathrm{laser}} &= \Omega_{\mathrm{L}}(\hat{\sigma}_{\mathrm{t}\uparrow}e^{\mathrm{i}\Delta\omega \mathrm{t}} + \hat{\sigma}_{\uparrow\mathrm{t}}e^{-\mathrm{i}\Delta\omega \mathrm{t}}) \\
&+ \sum_i \frac{A_i\Omega_{\mathrm{L}}}{\omega_{\mathrm{z}}}(\hat{I}^i_-\hat{\sigma}_{\mathrm{t}\downarrow}e^{\mathrm{i}(\omega_{\mathrm{t}}-\omega_{\mathrm{z}}-\omega_{\mathrm{L}})\mathrm{t}} + \mathrm{h.c.}) \qquad (7) \\
\tilde{H}_{\mathrm{rad}} &= \sum_k g_k(\hat{\sigma}_{\uparrow\mathrm{t}}\hat{a}^\dagger_k e^{\mathrm{i}(\omega_k-\omega_{\mathrm{t}})\mathrm{t}} + \mathrm{h.c.}) \\
&+ \sum_{i,k} \frac{A_i g_k}{\omega_{\mathrm{z}}}(\hat{I}^i_+\hat{\sigma}_{\downarrow\mathrm{t}}\hat{a}^\dagger_k e^{\mathrm{i}(\omega_k+\omega_{\mathrm{z}}-\omega_{\mathrm{t}})\mathrm{t}} + \mathrm{h.c.}) \qquad (8) \\
\tilde{H}_{\mathrm{ph}} &= \sum_q g_q\hat{\sigma}_{\mathrm{z}}\hat{b}_q e^{-\mathrm{i}\omega_q \mathrm{t}} + \mathrm{h.c.} \\
&+ \sum_{i,q} \frac{A_i g_q}{\omega_{\mathrm{z}}}\hat{I}^i_+\hat{\sigma}_-\hat{b}_q e^{\mathrm{i}(\omega_{\mathrm{z}}-\omega_q)\mathrm{t}} + \mathrm{h.c.} \qquad (9) \\
\tilde{H}_{\mathrm{OH}} &= \sum_i 2A_i\hat{I}^i_{\mathrm{z}}\hat{\sigma}_{\mathrm{z}} \qquad (10)
\end{aligned}$$

We find new terms such as hyperfine assisted coupling of the $|\downarrow\rangle \leftrightarrow |t\rangle$-transition to the laser field (second term in Eq. 7), hyperfine assisted spin-flip Raman-scattering (second term in Eq. 8) and co-tunneling/phonon-assisted hyperfine interaction (second term in Eq. 9). In the simulations we neglect laser coupling of the $|\downarrow\rangle \leftrightarrow |t\rangle$-transition due to the large detuning. The Hamiltonian in the interaction picture is given by $\tilde{H} = \tilde{H}_{\mathrm{coherent}} + \tilde{H}_{\mathrm{res\text{-}int}}$, where $\tilde{H}_{\mathrm{coherent}} = \tilde{H}_{\mathrm{laser}} + \tilde{H}_{\mathrm{OH}}$ and $\tilde{H}_{\mathrm{res\text{-}int}} = \tilde{H}_{\mathrm{rad}} + \tilde{H}_{\mathrm{ph}}$ the interactions with the reservoirs. The Master-equation for the reduced density operator of the combined electron-nuclei system in the Born-Markov approximation is given by

$$\frac{d\hat{\rho}_{\mathrm{S}}(t)}{dt} = -\frac{\mathrm{i}}{\hbar}[\tilde{H}_{\mathrm{coherent}}, \hat{\rho}_{\mathrm{S}}(t)] - \frac{1}{\hbar^2}\int_0^t dt' \mathrm{Tr}_{\mathrm{R}}\left\{[\tilde{H}_{\mathrm{res-int}}(t), [\tilde{H}_{\mathrm{res-int}}(t'), \hat{\rho}_{\mathrm{S}}(t)\otimes\hat{\rho}_{\mathrm{R}}(0)]]\right\} \qquad (11)$$

where $\hat{\rho}_{\mathrm{S}}$ and $\hat{\rho}_{\mathrm{R}}$ denote the system and reservoir density operator respectively. We trace out the electromagnetic field reservoir and the phonon degrees of freedom and find a Lindblad master equation $\hat{\rho}_{\mathrm{S}} = \hat{\mathcal{L}}\hat{\rho}_{\mathrm{S}}$. Heavy-light hole mixing induced spontaneous Raman scattering from the $|t\rangle$-state to the $|\downarrow\rangle$-state is added by a collapse operator with a rate γ_{hhlh}.

Finally we introduce two symmetric collapse operators $\sqrt{\gamma_{\mathrm{det}}}\hat{I}_+\hat{\sigma}_-$ and $\sqrt{\gamma_{\mathrm{det}}}\hat{I}_-\hat{\sigma}_+$ with a rate $\gamma_{\mathrm{det}} = \left(\frac{A/\sqrt{N}}{\omega_{\mathrm{Z}}}\right)^2\gamma_{\mathrm{spin}}(\Omega_L)$, originating from a resonant-absorption induced spin dephasing mechanism that is proportional to the stimulated absorption rate $\gamma_{\mathrm{spin}} \propto W_{\mathrm{abs}} = \Omega_{\mathrm{L}}^2\Gamma/(4\Delta\omega^2 + 2\Omega_{\mathrm{L}}^2 + \Gamma^2)$. This phenomenological electron spin dephasing rate γ_{spin} is not captured by the optical Bloch equations (that one would have obtained using $\hat{H}$ after tracing over the nuclear spin degrees of freedom) and is used as a fitting parameter in the simulations. We find that bi-directional DNSP is observable for a wide range of γ_{spin} values; the results plotted in Fig. 3E assumed $\gamma_{\mathrm{spin}} = \Gamma$ for $\Omega_L = \Gamma$

DOI: 10.1038/NPHYS1363

and $\Delta\omega = 0$. Prior experiments on DNSP also revealed the existence of optical excitation induced spin dephasing [3]. Possible sources of such dephasing or decay could include a laser absorption induced non-equilibrium phonon population in the neighborhood of the QD[4]. Remarkably, the spin measurement effected by resonant Rayleigh scattering, does not lead to direct hyperfine plus dephasing assisted flip-flop transitions due to a destructive quantum interference.

To obtain a tractable master equation for a large number of nuclei ($N \sim 1000$) we model the nuclear spin-system in the Dicke basis of collective spin states $|I, I_z\rangle$ which are characterized by their total angular momentum $I (0 \leq I \leq N/2)$ and its projection into the z-axis I_z. States with different I but identical I_z are weakly coupled by jump processes. The overall contribution of each I to the coupled dynamics is weighted by the number $D(I) = \begin{pmatrix} N \\ N/2 - I \end{pmatrix} - \begin{pmatrix} N \\ N/2 - I - 1 \end{pmatrix}$ of allowed permutation group quantum numbers associated with that total angular momentum.

Since all interactions between the QD electrons and the nuclei within our treatment based on the Born-Markov approximation are of incoherent nature, we assume that the nuclear density operator is diagonal, such that the total density operator can be written as

$$\hat{\rho}_{\mathrm{S}} = \sum_{I, I_z} P(I, I_z) \hat{\rho}_{\mathrm{QD}}(I, I_z) \tag{12}$$

With this assumption we calculate the matrix elements of the Liouvillian $\hat{\mathcal{L}}$. We finally solve the master equation in steady state for a large range of system parameters.

The relevant physical processes that determine the coupled electron-nuclear spin dynamics is depicted in Figure S3: as discussed in the main text, a competition between the Overhauser and reverse-Overhauser processes determine the degree and direction of nuclear spin polarization. Both processes are captured by our master equation formalism.

III. COMPETITION OF RATES: AN EXPLANATION OF BI-DIRECTIONAL NUCLEAR SPIN POLARIZATION

Three different processes (Overhauser, Reverse Overhauser and resident electron mediated decay) add to a detuning dependent polarization rate ($\frac{\mathrm{d}P}{\mathrm{dt}}$) of the nuclear spins. The electron mediated decay adds as a detuning-independent offset that changes with the nuclear spin polarization and limits the magnitude of nuclear spin polarization. Figure S4b illustrates the polarization rate as a function of effective laser detuning $\Delta\tilde{\omega} = \tilde{\omega}_{\mathrm{t}} - \omega_{\mathrm{L}}$ for a vanishing nuclear spin polarization. Energy shifts of the electron spin states due to a nuclear spin polarization are included in the effective trion transition energy $\tilde{\omega}_t$. The system locks to a to a condition where the effective polarization

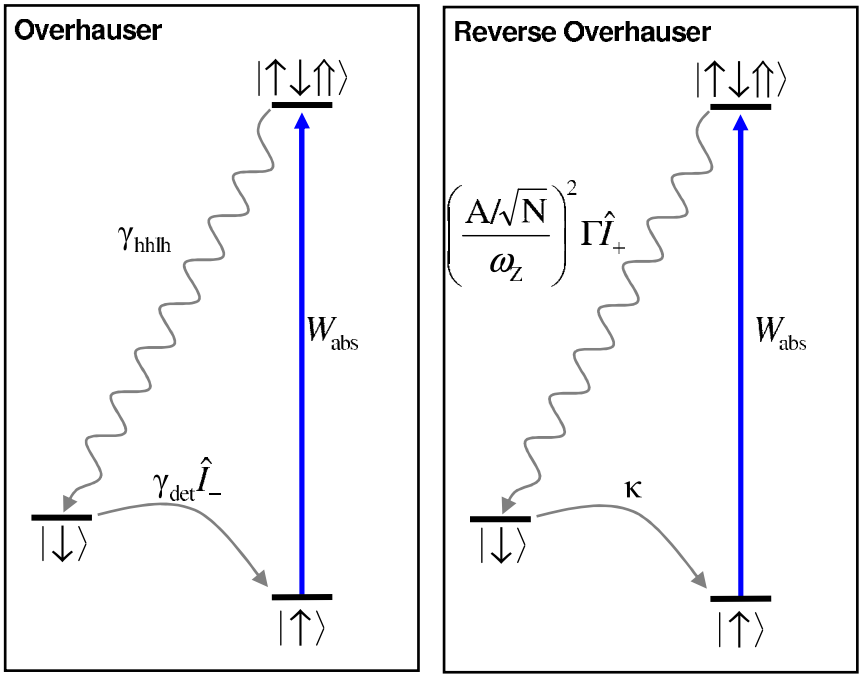

Figure 3: Schematic of the two competing nuclear spin pumping processes: the left panel depicts the process that polarizes the nuclear spins along the $-z$ axis (Overhauser-process). Photon absorption ($W_{\rm abs}$) followed by heavy-light-hole mixing induced spontaneous emission ($\gamma_{\rm hhlh}$) pumps the $|\downarrow\rangle$-state. A spin dephasing mechanism which we assume to be induced by resonant absorption (with rate $\propto W_{\rm abs}$) broadens the $|\uparrow\rangle$-$|\downarrow\rangle$ transition and enables direct hyperfine interaction between the electron and nuclei with a rate $\gamma_{\rm det}$. The right panel depicts the reverse Overhauser process. Hyperfine induced spin-flip Raman scattering ($\left(\frac{A/\sqrt{N}}{\omega_Z}\right)^2 \Gamma\hat{I}_+$) polarizes the nuclear spins along the +z axis. A is the homogeneous hyperfine coupling constant, N is the number of nuclei that the quantum dot electron interacts with and $\omega_{\rm Z}$ the Zeeman splitting of the electron states. Γ is the spontaneous emission rate from the trion state. The operator $\hat{I}_+(\hat{I}_-)$ increases(decreases) the angular momentum projection of nuclear spins along the z-axis by 1. The system is re-initialized by a spin-flip co-tunneling event with rate κ.

rate vanishes($\frac{{\rm d}P}{{\rm dt}}=0$). For $P=0$ this condition is satisfied for two detunigs $\Delta\tilde{\omega}=+\delta_{\mathbf{locking}}$ and $\Delta\tilde{\omega}=-\delta_{\mathbf{locking}}$, while only $\Delta\tilde{\omega}=+\delta_{\mathbf{locking}}$ is stable. When the laser is red-detuned by $\delta_{\rm L}$ from the stable point ($\Delta\tilde{\omega}=\delta_{\rm locking}+\delta_{\rm L}$) the reverse Overhauser process dominates ($\frac{{\rm d}P}{{\rm dt}}>0$) and nuclear spins are polarized along the +z axis. Due to the negative g-factor of the electron, the effective magnetic field produced by nuclei is along the -z axis. This process shifts the energy of the electron spin states until the locking condition $\Delta\tilde{\omega}=\delta_{\rm locking}$ is reached again and $\frac{{\rm d}P}{{\rm dt}}=0$ is achieved. The DNSP acts to ensure that the renormalized $\Delta\tilde{\omega}=\delta_{\rm locking}$ remains fixed and positive. Similarly, if the laser is blue detuned by a small amount, $\frac{{\rm d}P}{{\rm dt}}$ becomes negative and the Overhauser process polarizes the nuclear spins along the -z-axis. It should be noted that the laser detuning from the

DOI: 10.1038/NPHYS1363

bare trion resonance ($P = 0$) is irrelevant, to the extent that the system is within the dragging regime.

When we take nuclear spin decay into account (see Fig. S4d and S4e), we find that for $P > 0$ (i.e. nuclear spins polarized by the reverse-Overhauser effect) there are actually two stable points: one is slightly red detuned from the DNSP shifted resonance, and the other far blue detuned. However from our experiments we conclude that the system preferentially locks to a point close to the trion resonance where the absorption strength is close to its maximum. This behavior cannot be explained by the classical model depicted in Fig. S4. The master equation analysis shows that fluctuations in the Overhauser field variance are suppressed when the system locks close to the resonance while they remain large for large detunings. We tentatively argue that the system does not remain locked to the blue detuned stable point due to the fact that fluctuations are large for this condition. Once the system finds the red detuned stable point where absorption strength is close to its maximal value, its fluctuations are suppressed (see Figure 4 of the text) and the electron-nuclear spin system remains locked.

Since the decay of the nuclear spin polarization is proportional to the polarization, the total nuclear spin polarization rate can be written as

$$\frac{dP}{dt} = \alpha_{\mathrm{ROH}} W_{\mathrm{abs}} + \alpha_{\mathrm{OH}} W_{\mathrm{abs}}^2 - \gamma_{\mathrm{dec}} P. \tag{13}$$

The maximum degree of nuclear spin polarization that can be achieved by dragging is

$$P_{\mathrm{max}}^{-} \leq \frac{\alpha_{\mathrm{OH}} W_{\mathrm{peak}}^2 - \alpha_{\mathrm{ROH}} W_{\mathrm{peak}}}{\gamma_{\mathrm{dec}}} \tag{14}$$

where

$$W_{\mathrm{peak}} = \frac{\Omega_{\mathrm{L}}^2 \Gamma}{\Gamma^2 + 2\Omega_{\mathrm{L}}^2}. \tag{15}$$

Finally, we speculate that the asymmetry in the absorption recovery time is associated with the fact that for an initial large laser detuning, the reverse-Overhauser effect will first dominate and will lead to $P > 0$. This finite polarization will then ensure that the coupled electron-nuclear spin system has two stable points - one with low absorption and one with near-peak absorption (Fig. S4). For a blue detuned laser field, the system will then be partially stuck on the stable point with low absorption until fluctuations enable it to find the other stable point where fluctuations are suppressed. This will in turn lead to a slower absorption recovery time.

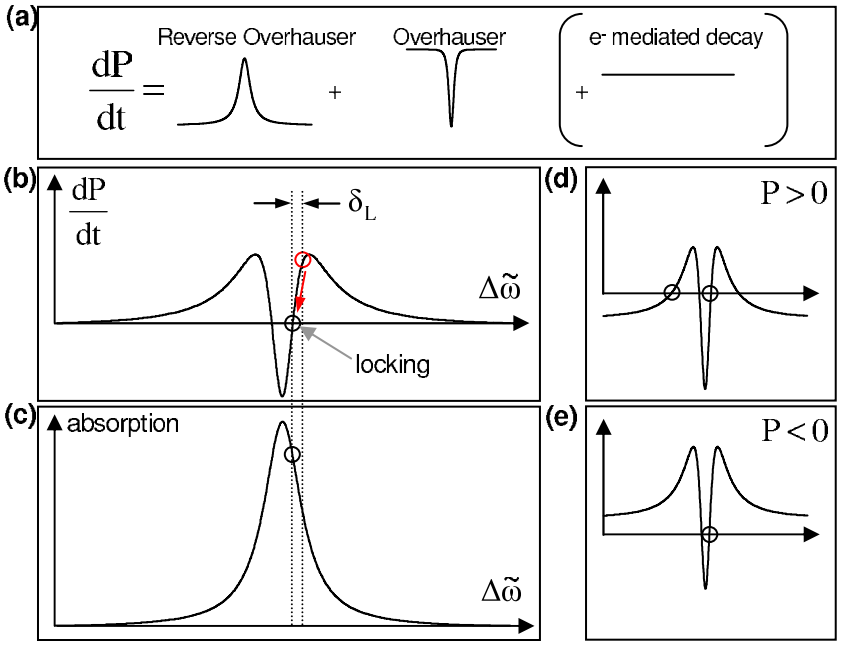

Figure 4: Competition of polarization rates **(a)** Composition of the effective polarization rate. (b) Polarization rate as a function of effective laser detuning $\Delta\tilde{\omega}$ ($P = 0$). The locking point ($\frac{dP}{dt} = 0$), where $\Delta\tilde{\omega} = \delta_{\text{locking}}$ is marked by the black circle. When the laser is red-detuned by δ_L from the locking point ($\frac{dP}{dt} > 0$, red circle), nuclear spins are polarized along the +z-axis thereby building up an effective magnetic field along the -z-axis ($g_e < 0$). This process shift the energy of the $|\uparrow\rangle$ until the locking-point is reached again (red arrow in (b)). (c) When $\Delta\tilde{\omega} = \delta_{\text{Locking}}$ the measured absorption is close to its maximum (black circle). (d) $\frac{dP}{dt}$ for $P > 0$. The two stable points are highlighted by black circles. (e) $\frac{dP}{dt}$ for $P < 0$. The only stable point is highlighted by a black circle.

[1] Alen, B. *et al.* Stark-shift modulation absorption spectroscopy of single quantum dots. *Appl. Phys. Lett.* **83**, 2235 (2003).

[2] Kroner, M. *et al.* Optical Detection of Single-Electron Spin Resonance in a Quantum Dot. *Phys. Rev. Lett.* **100**, 156803 (2008).

[3] Maletinsky, P. *et al.* Nonlinear dynamics of quantum dot nuclear spins. *Phys. Rev. B* **75**, 035409 (2007).

[4] Flindt, C. *et al.* (private communication).